

# Optics near Kerr black holes: spectra of advection dominated accretion flows.

M. Jaroszyński and A. Kurpiewski

Warsaw University Observatory, Al. Ujazdowskie 4, 00-478 Warsaw, Poland

August 21, 2019

**Abstract.** We investigate advection dominated, transonic accretion flows in the vicinity of a Kerr black hole. We take into account all relativistic effects in the dynamics of the flow and in the propagation of light. We assume the matter to be weakly magnetized and cool via the thermal synchrotron and Bremsstrahlung radiation. We include also the effects of Comptonization. We calculate the spectra of radiation as seen by observers located at different positions relative to the equatorial plane of the disk. The radiation emitted by the accreting matter is anisotropic and observers near the equatorial plane register a higher energy flux. This effect is more pronounced in the case of slowly rotating black holes. We calculate also the shape of a hypothetical gamma line, which may be produced by the thermonuclear reactions in the inner part of the flow. The line is strongly broadened, but the fact that the flow is quasi-spherical removes the two-peak shape of the line seen in the spectra emitted from thin, Keplerian disks. The kinematics of the advection dominated flows is not unique (as opposed to Keplerian disks or spherical free-fall) and it would probably be difficult to find strong limits on source models using the spectral observations.

**Key words:** accretion processes - radiation mechanisms: non-thermal -relativity

considered by Katz (1977). Spherical accretion with advection has been investigated by Begelman (1978, 1979). The role of advection in disk-like accretion has been studied by Begelman & Meier (1982), Abramowicz, Lasota & Xu (1986) and Abramowicz et al. (1988) for configurations with substantial optical and geometrical thickness. These models are sometimes called *slim accretion disks*. The advection of heat makes the energy conservation nonlocal, as opposed to thin disks, and thus influences their structure, but due to the substantial optical thickness, has no prominent influence on their spectrum. Another branch of accretion flows has been discovered by Narayan & Yi (1995) and Abramowicz et al. (1995). Flows belonging to this class are extremely optically thin and have low accretion rate. Because of the low radiation efficiency, the gas can heat up to near virial temperatures. For this reason the flow becomes quasi-spherical and pressure gradients play an important role in the gas dynamics. The radial and azimuthal velocities can have the same order of magnitude. These are the main characteristics of ADAFs. Because of their high temperatures ADAFs produce X-rays in a natural way. On the other hand the effectiveness of accretion is low, because almost all the thermal energy goes under the horizon with accreting matter. These properties make ADAFs possible explanation for some X-ray sources and such models have been proposed (Narayan 1996; Lasota et al. 1996; Narayan, McClintock & Yi 1996; see also Rees, 1982).

The general properties of the advective flows have been obtained with the help of Newtonian or pseudo-newtonian (Paczyński & Wiita 1980) description of the background gravitational field. Lasota (1994), Abramowicz et al. (1996, hereafter ACGL) and Abramowicz, Lanza & Percival (1997, hereafter ALP) have obtained a self-consistent system of equations describing the accretion flows in the Kerr spacetime. All these papers use the *vertical averaging* to obtain a set of ordinary differential equations to describe the flow. The form of equations resembles the equations for an accretion disk, but some properties of the quasi-sphericity are taken into account (see ALP).

## 1. Introduction

The advection dominated accretion flows (ADAFs) have recently become an interesting alternative to the traditional thin accretion disks (Shakura & Sunyaev 1973; Novikov & Thorne 1973). The disk model with a two temperature, optically thin and hot inner region has been proposed by Shapiro, Lightman & Eardley (1976). The spherical accretion flow, which cannot cool, because the radiation is trapped and advected with matter, has been

The properties of ADAFs in fully relativistic treatment have been also investigated by Peitz & Appl (1996). All these papers investigate mainly the flow dynamics and are concentrated on its properties and their dependence on parameters such as viscosity parameter  $\alpha$  and the dimensionless accretion rate  $\dot{m}$ .

We are interested in the radiation processes and spectra emitted by ADAFs in the Kerr spacetime. The main reason of our investigation is to get a fully self-consistent, relativistic description of the radiation from the advective flows. The gas has the highest temperatures near the horizon, so the combined effects of ray deflection, Doppler shifts and gravitational redshift may influence the high energy end of the spectrum, at least quantitatively. Since the flow is optically thin, the observer may have a chance to see the matter on the other side of the black hole approaching the telescope with relativistic speed; in some cases this should lead to the beaming of radiation and substantial increase of the surface brightness. The possibility and importance of such effects should be investigated.

Since we are mostly interested in the propagation of light, we are not going to investigate the hydrodynamics of the flow in detail. To get rough solutions of the hydrodynamic equations we use an approximate treatment, neglecting the cooling. Thus the most time consuming part of the calculations is decoupled from the equations of motion. For a simple equation of state the structure of the flow (i.e. the profile of the angular momentum, radial velocity of matter and the speed of sound) depends only on the viscosity parameter  $\alpha$  and the values of the specific angular momentum and energy of matter at the horizon. The matter density depends on the above variables and scales with the accretion rate. Using the same solution of the equations of motion one is able to get models with different accretion rate. Inspection of the solutions of the hydrodynamic equations of Chen, Abramowicz & Lasota (1997), which include cooling, shows that dependence on the accretion rate is weak, at least in the inner part of the flows.

In the next Section we present the system of equations, which we use to model the accretion flow and rays tracing. We also describe the approach to radiation processes within the flow. In Sec.3 we present the results of calculations, showing the brightness profiles of our sources, their spectra, and luminosity dependence on the observer inclination angle. The discussion follows in the last Section.

## 2. The model

### 2.1. The accretion flow

We investigate the stationary flow of matter and the propagation of light in the gravitational field of a rotating Kerr black hole using the Boyer-Lindquist coordinates  $t, \phi, r, \theta$  and the metric components  $g_{ab}(r, \theta)$  as given by Bardeen (1973). We follow the  $(-, +, +, +)$  signature convention.

When dealing with the flow we use the metric tensor with components evaluated at the equatorial plane ( $\theta = \pi/2$ ). We use geometrical units, so the speed of light  $c \equiv 1$  and the mass of the hole  $M \equiv 1$ . (Later we use  $c$  for the speed of sound.) The Kerr parameter  $a$  ( $0 \leq a < 1$ ) gives the black hole angular momentum in geometrical units. We use the Einstein summation convention, where needed and a semicolon for the covariant derivative. The normalization of four velocity with the chosen metric signature reads  $u^a u_a = -1$ .

The system of equations we use follows in general ACGL. Since we are neglecting the cooling processes at this stage, and treat the accretion flow in the disk approximation, two components of velocity and the speed of sound  $c$  given as functions of radius, fully describe the dynamics. We use the angular velocity  $\Omega$  and the physical radial velocity  $V$  as measured by locally nonrotating observers as main kinematic variables (compare ACGL). After the *vertical averaging* the velocity perpendicular to the equatorial plane is neglected ( $u^\theta \equiv 0$ ) and other components of the four velocity are given as:

$$u^t = \frac{1}{\sqrt{1 - V^2} \sqrt{-g_{tt} - 2\Omega g_{t\phi} - \Omega^2 g_{\phi\phi}}} \quad (1)$$

$$u^\phi = \Omega u^t \quad (2)$$

$$u^r = \frac{1}{\sqrt{g_{rr}}} \frac{V}{\sqrt{1 - V^2}} \quad (3)$$

We shall later use the two temperature plasma to describe the cooling processes. In the hottest and most interesting part of the flow the pressure of the nonrelativistic ions,  $p = n_i k T_i$ , where  $n_i$  is ion concentration,  $T_i$  their temperature and  $k$  the Boltzmann constant, dominates. The isothermal sound speed can be defined as

$$c^2 = \frac{k T_i}{m} \quad (4)$$

where  $m$  is the average ion mass, so one has  $p = \rho_0 c^2$ , where  $\rho_0$  is the rest mass density. The specific enthalpy  $\mu$  is given as:

$$\mu \equiv \frac{\epsilon + p}{\rho_0} = 1 + \frac{5}{2} c^2 \quad (5)$$

where  $\epsilon$  is the total (rest mass plus thermal) energy density. The above formula implicitly assumes that the matter can be treated as the ideal, nonrelativistic gas.

The mass conservation equation relates the mass accretion rate  $\dot{M}$ , with the radial velocity and the surface rest mass density  $\Sigma$  (ACGL):

$$\dot{M} = -2\pi \Sigma \sqrt{\Delta} \frac{V}{\sqrt{1 - V^2}} \quad (6)$$

where  $\Delta(r) \equiv r^2 - 2r + a^2$  is one of the functions defining the metric. On the horizon one has  $\Delta(r_h) = 0$  and  $V = -1$  (see ACGL), but the ratio  $\Delta/(1 - V^2)$  remains finite and is related to the derivative of radial velocity at  $r = r_h$ . Thus the surface mass density remains finite everywhere and using mass conservation one can substitute for  $\Sigma$  in other equations.

The rest mass density of matter can also be replaced in the equations with the help of the so called *vertical hydrostatic equilibrium equation*, which reads:

$$\frac{dp}{dz} = -\mu\rho_0 g_{,z} z \quad (7)$$

where  $g_{,z}$  represents the gravitational tidal forces as measured at the equatorial plane by an observer comoving with the fluid, and  $z$  is his coordinate in this direction. We use the prescription of ALP for the tidal forces, so the expression remains finite at the horizon:

$$g_{,z} = \frac{u_\phi^2 - a^2(u_t^2 - 1)}{r^4} \equiv \frac{\rho_*^2}{r^4} \quad (8)$$

For an optically thin medium we assume the temperature to be approximately constant in the vertical direction. The integration of the equation gives the density distribution:

$$\rho_0(r, z) = \rho_0(r, 0) \exp\left(-\frac{1}{2} \frac{z^2}{H^2}\right) \quad (9)$$

where

$$H^2 = \frac{c^2 r^4}{\mu \ell_*^2} \quad (10)$$

is the scale height. The form of the above expression shows, that  $c^2/\mu$  has the physical meaning of the square of the speed of sound. Integration of the density distribution over the disk thickness gives  $\Sigma = \sqrt{2\pi}\rho_0 H$ . Knowing the surface mass density and the scale height one can substitute for the rest mass density.

We are neglecting transport of heat within the fluid, but we do include the processes due to the shear viscosity, so the energy momentum tensor has the form (Novikov & Thorne 1973):

$$T_b^a = (\epsilon + p)u^a u_b + p\delta_b^a - 2\eta\sigma_b^a \quad (11)$$

where  $\delta_b^a$  is the Kronecker delta,  $\eta$  the dynamical viscosity, and  $\sigma_b^a$  the shear tensor:

$$\sigma_{ab} = \frac{1}{2}(u_{a;i}h_b^i + u_{b;i}h_a^i) - \frac{1}{2}\Theta h_{ab} \quad (12)$$

The equations of motion for the disk are written under the assumption that the velocity in the vertical direction can be neglected and all variables are evaluated in the equatorial plane. The motion is effectively two dimensional and all tensors should be treated as acting in three dimensional

space time. The projection tensor  $h_b^a = \delta_b^a + u^a u_b$  and its  $3^d$  trace  $h_a^a = 2$ . This is why we use the factor  $1/2$  instead of conventional  $1/3$  in front of the term including the velocity expansion  $\Theta = u_{;a}^a$  in the definition of the shear tensor.

The projected equation of motion,  $h_r^b T_{b;a}^a = 0$  takes the form:

$$\frac{V^2 - c^2/\mu}{1 - V^2} \frac{V'}{V} + 2\frac{c^2}{\mu} \frac{c'}{c} = \frac{1}{2} \frac{c^2}{\mu} \frac{\Delta'}{\Delta} + \frac{1}{2}(1 - V^2)(u^t)^2 (g'_{tt} + 2\Omega g'_{t\phi} + \Omega^2 g'_{\phi\phi}) \quad (13)$$

where the primes denote the derivatives relative to  $r$ . We neglect the terms related to the viscosity in this equation, which is the usual simplification (ACGL, Peitz & Appl 1997).

Projecting the equation of motion into the comoving reference frame,  $u^b T_{b;a}^a = 0$  leads to the energy conservation equation in the form (Novikov & Thorne 1973, ACGL):

$$\rho_0 T u^a \nabla_a S = 2\eta\sigma^2 \quad (14)$$

where  $S$  is the entropy of the fluid per unit mass and the derivative is in fact relative to the proper time. In the stationary, axially symmetric case  $u^a \nabla_a = u^r \partial_r$ . The entropy of an ideal gas is given as:

$$S = \frac{k}{m} \left( \frac{3}{2} \ln T - \ln \rho_0 \right) + const \quad (15)$$

For the viscosity in the  $\alpha$ -disk approximation one has:

$$\eta = \alpha\rho_0 \frac{c}{\sqrt{\mu}} H = \alpha\rho_0 \frac{c^2 r^2}{\mu \ell_*} \quad (16)$$

where we use the expression for the sound speed with the proper physical meaning. The equation for the entropy gradient can now be expressed as:

$$\frac{V'}{V} + 3\frac{c'}{c} + \frac{H'}{H} = -\frac{1}{2} \frac{\Delta'}{\Delta} - \frac{2\alpha r^3}{\mu \ell_*} \sqrt{\frac{(1 - V^2)}{\Delta V^2}} \sigma^2 \quad (17)$$

where the radial derivative of the scale height is still to be expressed via the gradients of the angular and radial velocities and the speed of sound.

The symmetries of the Kerr metric imply the energy and angular momentum conservation equations for the fluid in the form  $T_{t;a}^a = 0$ ,  $T_{\phi;a}^a = 0$ . After integrating over  $r$  and vertically averaging one has:

$$\frac{\dot{M}}{2\pi} (\mu u_\phi - \mu^0 u_\phi^0) + 2\alpha r \Sigma \frac{c^2 r^2}{\mu \ell_*} \sigma_\phi^r = 0 \quad (18)$$

$$\frac{\dot{M}}{2\pi} (\mu u_t - \mu^0 u_t^0) + 2\alpha r \Sigma \frac{c^2 r^2}{\mu \ell_*} \sigma_t^r = 0 \quad (19)$$

where the superscript 0 denotes variables as measured on the horizon. We define the specific energy of the fluid as  $\mathcal{E} = -\mu u_t$  and its specific angular momentum as  $\mathcal{L} = \mu u_\phi$ . We also use the kinematic specific angular momentum  $\ell = -u_\phi/u_t$ . Combining the upper equation multiplied by  $\mathcal{E}$  with the lower equation multiplied by  $\mathcal{L}$  we get:

$$\frac{\alpha c^2 r^3}{\ell_*} (2\sigma_t^r u_\phi - 2\sigma_\phi^r u_t) = -\sqrt{\frac{\Delta V^2}{1-V^2}} \mathcal{E} \mathcal{E}_0 (\ell - \ell_0) \quad (20)$$

The combination of the shear tensor components, which we use, contains the angular velocity gradient but not the radial velocity gradient:

$$2\sigma_t^r u_\phi - 2\sigma_\phi^r u_t =$$

$$\frac{\Delta (u^t)^2}{1-V^2} \Omega' + \frac{V^2 [\ell g'_{tt} + (1 + \Omega \ell) g'_{t\phi} + \Omega g'_{\phi\phi}]}{(1-V^2)^2 (1 - \Omega \ell)} \quad (21)$$

Thus the equation for  $\Omega$  is obtained. It has a boundary condition at the horizon  $\Omega = \omega$ , where  $\omega = -g_{0\phi}/g_{\phi\phi}$  is the angular velocity of the dragging of inertial frames.

We solve the equations for  $V$ ,  $c$  and  $\Omega$  by iterations. We start from a solution with subkeplerian rotation, which asymptotically (far from the hole) becomes a selfsimilar solution as described by Narayan & Yi (1994). We postulate the position of the sonic radius  $r_s$  and the value of the angular momentum at the horizon  $\ell_0$  and, using the angular velocity distribution from the initial guess (and later on from the previous iteration), we solve the equations for the radial velocity and the speed of sound. These equations are easy to integrate if one starts from the sonic point. For a given angular velocity distribution, in particular knowing its value at the sonic point  $\Omega_s$ , we find the values of the other two variables  $V_s$ ,  $c_s$  from the regularity conditions. The boundary condition on the horizon ( $V = -1$ ) is always met. The value of specific energy on the horizon results from the solution and is iterated. Next we solve the equation for the angular velocity starting from the horizon outward, which gives a new angular momentum distribution. The expression for the square of the shear ( $\sigma^2$ ) contains derivatives of the angular and radial velocities, and is rather complicated, including the derivatives in the second power. Using Eq.(12) we calculate the shear tensor from the “previous iteration” and substitute it into Eq.(17).

Not all postulated  $(r_s, \ell_0)$  pairs lead to solutions which can be continued from the horizon to infinity, but the iterations just described are so fast that checking many of them is easy. For a given angular momentum of the black hole we find the *best* parameters, for which the solution can be smoothly joined with the selfsimilar solution far away.

For the purpose of investigating the emitted spectra we choose examples of ADAF solutions in Kerr metric with

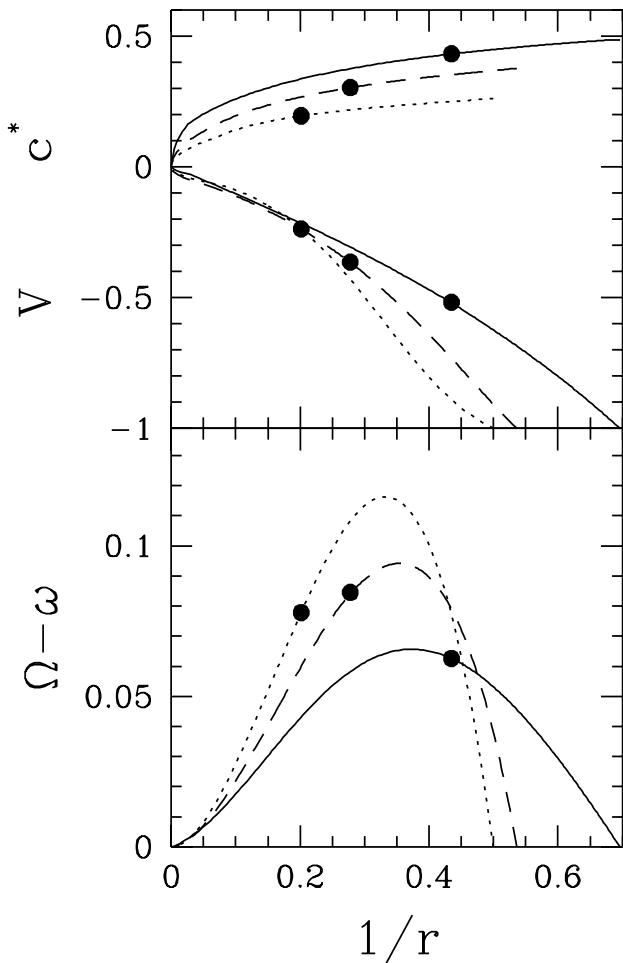


**Fig. 1.** Sample models of ADAFs. On the upper plot we show the radial velocity of the flow  $V$  (negative) and the sound speed  $c^* \equiv c/\sqrt{\mu}$  as functions of  $1/r$  for our three models in the Kerr metric with angular momentum  $a = 0$  (dotted line),  $a = 0.5$  (dashed line) and  $a = 0.9$  (solid line). The locations of the sonic points are shown as large dots on the lines. On the lower plot we show the angular velocity distribution  $\Omega - \omega$ , using the same conventions.

angular momentum  $a = 0, 0.5$  and  $0.9$ . We use the viscosity parameter  $\alpha = 0.1$ . For the Schwarzschild case the position of sonic radius and the value of the angular momentum on the horizon are in good agreement with Chen et al. (1997), who use the pseudo-Newtonian potential to describe gravity. The profiles of the sound speed and radial and angular velocities for our solutions are shown on Fig.1.

### 2.2. Radiation processes in the disk

We use two temperature plasma to describe radiation processes and local spectra in the disk. For given ion temperature  $T_i$ , scale height  $H$  and surface mass density  $\Sigma$  (Section 2.1.) we determine electron temperature by tak-

ing into account the detailed balance of their heating and cooling. We divide the disk into the coaxial cylindrical layers and treat them separately. We imagine each of the annuli to be cut from a plane parallel layer with constant temperature and the density concentrated toward the midplane according to Eq(9). We follow here the description of heating and cooling processes presented by Narayan & Yi (1995) and also by Esin et al. (1996) [and references therein]. They consider the energy transfer from ions to electrons via Coulomb collisions and cooling of electrons by synchrotron radiation, inverse Compton process and bremsstrahlung emission. They ignore the presence of  $e^+e^-$  pairs but as Björnsson et al. (1996) showed, the role of  $e^+e^-$  pairs in the structure of ADAF is not significant.

For calculated electron temperature we can model the local continuum emission per unit area from surface of each annulus. We assume that molecular weights of ions and electrons are  $\mu_i = 1.29$  and  $\mu_e = 1.18$ , and the density of magnetic field is parameterized by the ratio of gas pressure to total pressure  $\beta$ . In our calculations we ignore the radiation pressure, so the total pressure is the sum of gas pressure and magnetic field pressure. We use the approximate formulae of Esin et al. (1996) to calculate synchrotron spectrum and formulae of Jones (1968) to model the inverse Compton scattering of synchrotron photons. The method of approximate computation of bremsstrahlung spectrum is given in Svensson (1982) [and references therein]. We include the frequency averaged Comptonization of bremsstrahlung photons in the energy balance, but we neglect this process in the calculation of the spectrum, since it is very time consuming and its contribution to the resultant spectrum is not significant.

Figure 2 shows the continuum emission calculated for four annuli of radii  $r/r_g = 1.5; 10; 100; 1000$ , (where  $r_g = GM/c^2$  is the gravitational radius) and for the following parameters:  $M/M_\odot = 3.6 \cdot 10^7$ ,  $\dot{M}/\dot{M}_{Edd} = 0.016$ , corresponding to  $1.5 \cdot 10^{-3} M_\odot \text{yr}^{-1}$ ,  $\alpha = 0.1$  and  $\beta = 0.95$ . Such parameters have been chosen by Lasota et al. (1996) to model the spectral features of the nucleus of active galaxy NGC 4258, which they treat as a superposition of ADAF and a standard accretion disk. We show the hottest of our models, which has  $a = 0.9$ .

The importance of the Compton scattering depends on the total optical depth of the disk and, strictly speaking, is not a local process. In the following part we neglect this fact. The bremsstrahlung emission is a two body process and, under the assumption of constant temperature in vertical direction, we assume its rate to be proportional to the square of the density ( $\sim \rho^2$ ). Similarly the synchrotron emission, being proportional to the product of electron density and magnetic pressure, which has a constant ratio to the gas pressure and density, is also proportional to the square of the electron concentration. The rate of the Compton process depends on the electron concentration and the density of the radiation field. The latter one de-

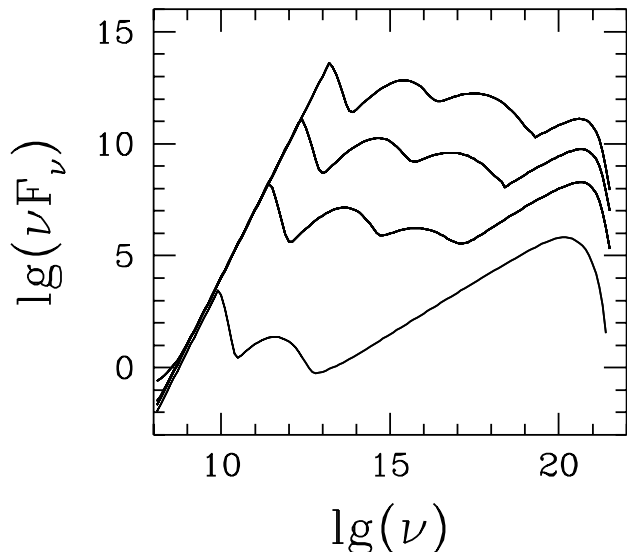


**Fig. 2.** Continuum emission per unit area from four annuli of radii  $r/r_g = 1.5; 10; 100; 1000$  (reading from highest line down) for parameters:  $M/M_\odot = 3.6 \cdot 10^7$ ,  $\dot{M}/\dot{M}_{Edd} = 0.016$ , corresponding to  $1.5 \cdot 10^{-3} M_\odot \text{yr}^{-1}$ ,  $\alpha = 0.1$ ,  $\beta = 0.95$ , and  $a = 0.9$ . The left peak of each curve is due to synchrotron radiation, the right one is due to bremsstrahlung emission and two peaks between them are due to the Compton scattering of synchrotron photons.

pends on the optical depth for scattering measured to the disk surface. Thus for this process the proportionality to the square of the matter density does not hold, but the decline toward the surface is also present and should have similar character. We use the following, simplified formula for the volume emissivity from the disk:

$$j(\nu) = \sqrt{\frac{2}{\pi}} \frac{F(\nu)}{\pi H} \exp\left(-\frac{z^2}{H^2}\right) \quad (22)$$

The flux here is the total energy emitted from the unit surface of the disk as usually used in this context. The emissivity  $j(\nu)$  is defined per one steradian and hence the integration of the above formula from the equatorial plane to infinity would give  $F(\nu)/\pi$ .

Our formalism described in the next subsection allows for the calculation of the source spectrum regardless of the nature of the radiation processes in the disk as long as the matter remains transparent to the radiation. We consider also the shape of the emission line, which may be used for testing the velocity field in the flow. We follow the idea of Narayan & Yi (1996), who consider the spallation process leading to the lithium and beryllium production. As shown by Kozlovsky & Ramaty (1974) some of the nuclei are produced in the excited state and emit  $\gamma$ -ray lines at 478 and 431 keV. The emissivity is proportional to the rate of production. Following closely Narayan & Yi (1996) we assume that there is a threshold energy 8.5 MeV for

the  $\alpha$ - $\alpha$  reaction to occur and we assume the cross-section to be inversely proportional to the energy of interacting particles  $\sigma \sim E^{-2} \sim c^{-4}$  (for  $c \geq c_{\text{threshold}}$ ). We use here the typical thermal energy of the  $\alpha$  particles instead of energy distribution averaging. The relative velocity of interacting particles is proportional to the thermal energy, and their concentration to the matter density. The width of the line results from the thermal motion of  ${}^7\text{Li}$  ions; they are slower than other particles because of the higher mass, and including the  $\sqrt{2}$  factor in the definition of the line width, we get:

$$\frac{\Delta\nu}{\nu_0} = 1.1c \quad (23)$$

where  $\nu_0$  is the line frequency and the mean ion mass  $1.29m_H$  of the matter containing 70% of hydrogen has been assumed in the calculation. Taking all the factors into account we obtain the formula for the line volume emissivity up to a constant factor:

$$j(\nu) \sim \frac{\rho^2 \exp\left(-\frac{(\nu-\nu_0)^2}{(\Delta\nu)^2}\right)}{c^3 \Delta\nu} \quad (24)$$

where the density is obtained from Eq.(9), and the formula is valid only for the sound velocity over the threshold.

### 2.3. Geometrical optics

We use the backward ray shooting method (Luminet 1979; Jaroszyński 1993) to obtain the spectrum of the electromagnetic radiation from the configuration. The intensity of radiation  $I(\nu_0)$  coming to a far observer at the frequency  $\nu_0$  along any ray is given as:

$$I(\nu_0) = \int_{\text{ray}} \frac{\nu_0^3}{\nu^3} j(\nu) dl_{\text{prop}} \quad (25)$$

where  $j(\nu)$  is the emissivity per unit volume, and  $dl_{\text{prop}}$  is the proper length differential as measured in the frame comoving with matter. The emission frequency  $\nu$  is given as:

$$\nu = \frac{u^a p_a}{p_0} \nu_0 \quad (26)$$

where  $u^a$  is the matter four velocity,  $p_a$  is the photon four momentum, and  $p_0$  - the photon energy in BL frame, which is conserved. This is the usual redshift (or blueshift) formula.

We find the null geodesics in the Kerr metric using the quadratures of Hamilton-Jacobi equation (Bardeen 1973). This method is faster, and more importantly, has a better accuracy as compared with the solution of ordinary differential equations along the trajectories.

Following many rays coming to an observer from the vicinity of the hole makes it possible to produce a map of the surface brightness of the source. Since the hottest part

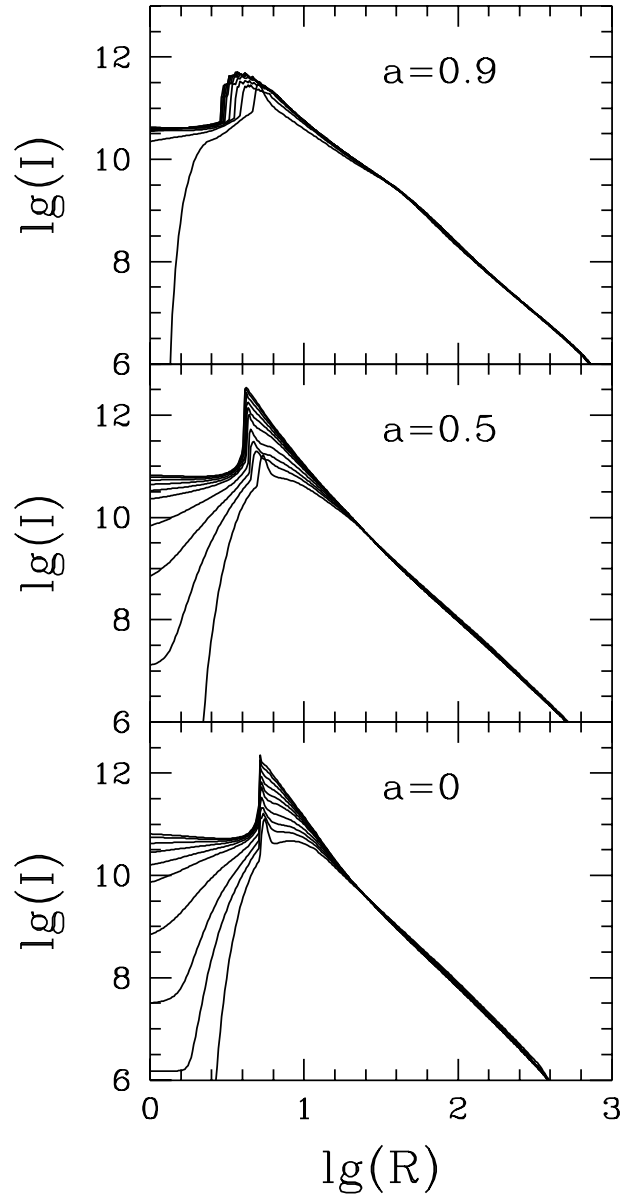


**Fig. 3.** Bolometric brightness profiles as seen by observers at the angles  $\theta = 5^\circ$  to  $85^\circ$ , bottom to top. The radius is in geometrical units, the brightness in c.g.s. units. The three plots correspond to the three models as indicated.

of the source is close to the hole, we probe the radiation intensity in rings centered on the hole with logarithmic distribution of radii. Thus the central parts are investigated with greater accuracy. A useful characteristic of the source is its radial surface brightness profile, as seen by a distant observer, obtained by integration over frequency and azimuthally averaging:

$$I(\xi) = \frac{1}{2\pi} \int_0^{2\pi} d\vartheta \int_0^\infty d\nu_0 I_{\nu_0}(\xi, \vartheta) \quad (27)$$

where  $\xi$  and  $\vartheta$  are the observer cylindrical coordinates on the sky. The length corresponding to the angle  $\xi$ , measured at the source, is  $R \equiv \xi D$ , where  $D$  is the distance to the source. The flux of radiation from the source as measured by an observer is given as:

$$F(\nu_0) = \int d\xi \int \xi d\vartheta I_{\nu_0}(\xi, \vartheta) \quad (28)$$

and implicitly depends on the observer location.

### 3. Results

We have made ray shooting calculations for observers at inclination angles  $\theta = 5^\circ, 30^\circ, 40^\circ, 50^\circ, 60^\circ, 65^\circ, 70^\circ, 75^\circ, 80^\circ$  and  $85^\circ$  as measured relative to the rotation axis, for the three models of ADAF in three background metrics with the Kerr parameter values  $a = 0, 0.5$  and  $0.9$ . In ray tracing we include only the radiation from a sphere of the radius  $r = 10^3 r_g$ . We do not include any other source components, as a thin Keplerian disk or a dust torus.

In Fig.3 we show the source surface brightness profiles as seen by observers at different inclinations. The relatively low surface brightness in the centre corresponds to rays, which traverse only the matter in front of the horizon. The densest and hottest part of the matter (close to the horizon) is receding from the observer, which also works as to decrease the observed brightness. The abrupt jump to higher surface brightness corresponds to rays which pass close to the hole. These rays spend relatively long time in the innermost part of the flow due to the bending. Some of them may be tangent to matter trajectories in isolated points. Doppler boost and relative increase in optical depth (which remains much lower than unity) both work as to increase the surface brightness. The dependence on the inclination angle is better pronounced for the low angular momentum black holes. The surface brightness is higher, when the source is watched from the vicinity of the equatorial plane.

The bolometric flux is also higher for observers close to the equatorial plane. As can be seen in Fig.4, the effect is moderate for the fast rotating hole (about 70% increase in flux measured at the equator as compared to the pole). For slowly rotating holes ( $a = 0.5$  or  $a = 0$ ) the source seen from the equatorial plane seems to be brighter by a factor 4.

The shape of the continuum spectra from our models is not considerably changed by the relativistic effects in the ray propagation. As seen on Fig.5 the spectra are shifted vertically, when the observer approaches the equatorial plane. The simultaneous shift to higher frequencies is very weak.

The line profiles are obtained with the help of the same calculation scheme, but the volume emissivity of matter given in Eq.(22) is replaced by Eq.(24). The lines are appreciably broadened. The mechanism of line formation which we use (spallation reactions leading to the pro-

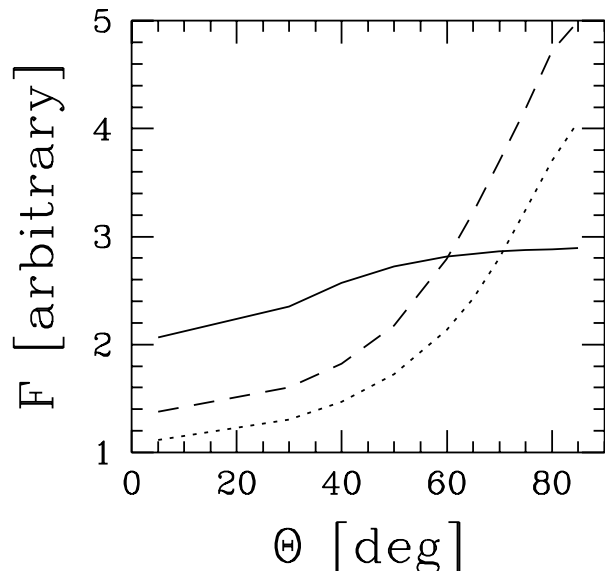


**Fig. 4.** The dependence of the observed total bolometric flux from the source on the observer inclination relative to the axis of rotation. We use the bolometric flux from our Schwarzschild model ( $a = 0$ ) as seen by an observer on the rotation axis as the unit of flux. The dotted line corresponds to the nonrotating hole ( $a = 0$ ), the dashed line to the case  $a = 0.5$  and the solid line to  $a = 0.9$ .

duction of lithium and beryllium nuclei in excited state), gives the lines which are broadened by thermal motion of the hot gas. The effects in light propagation (Doppler and gravitational shifts) are superimposed on the natural line broadening. As can be seen on the plots, these combined effects produce profiles without the characteristic two-peak structure as in the case of Keplerian disk (Hameury, Marck & Pelat 1994). Such two-peak structure is present in the spectra of the maximal surface brightness rings (compare Fig.3), but the light from these parts of the sources cannot be observed separately by a distant observer. Superposition of the spectra from all the rings removes the effect, but some traces of it can be seen in the spectra of our  $a = 0$  and to lesser extent  $a = 0.5$  models.

### 4. Discussion and conclusions

Our system of equations describing the relativistic advection dominated accretion flow onto a Kerr black hole is based on the ACGL and ALP papers but there are few differences. We use all the terms related to the radial and azimuthal motion of matter in the expression for shear, which is responsible for heat dissipation. We also combine the equations for energy and angular momentum conservation to get the equation for the angular momentum gradient, which does not contain gradients of radial velocity. (ACGL neglect such terms). We neglect the viscous forces in the equation for radial momentum balance; this approximation is also used by ACGL). We take into account

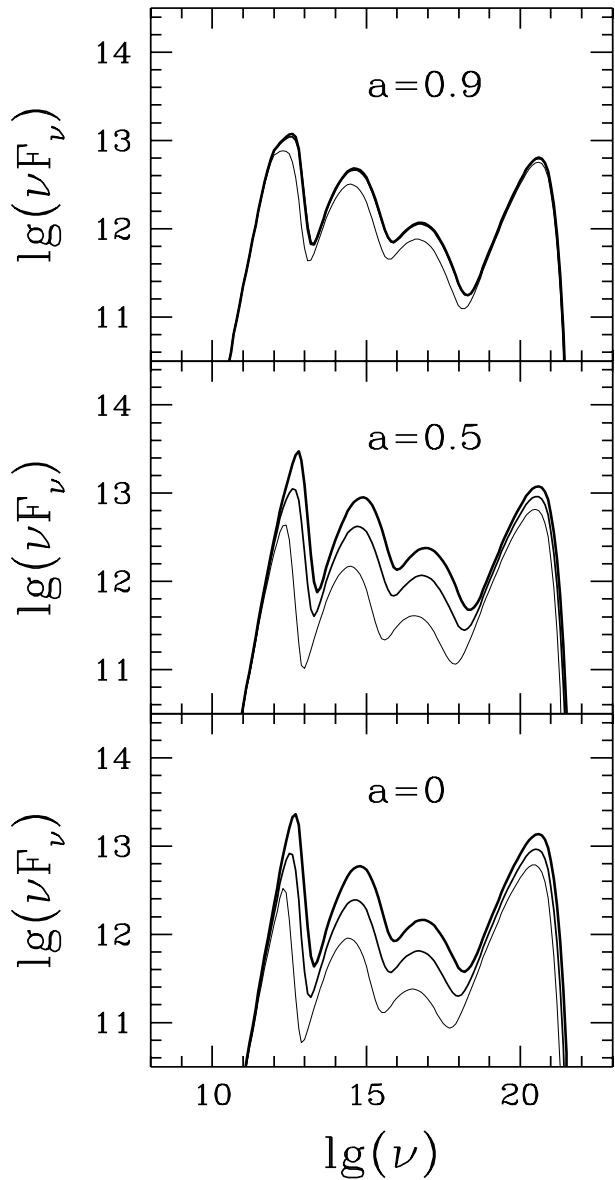


**Fig. 5.** The spectra of our models for observers at inclinations  $\theta = 5^\circ$  (thin solid lines),  $60^\circ$  (medium lines), and  $85^\circ$  (thick lines). The three panels correspond to the three models as indicated. The flux units are arbitrary.

the contribution of the thermal energy to the total energy density introducing the specific enthalpy  $\mu$  into our equations. Our description is however limited to the equation of state for an ideal, nonrelativistic gas. This approximation is reasonable, since the thermal energies of ions and electrons do not exceed their rest energies. The contribution to pressure of the magnetic field is low (5%) and does not limit the validity of the ideal gas approximation.

The most serious problem in our approach (and in other descriptions of ADAF in the frame of vertically averaged disk structure) is the fact, that the flow is not limited

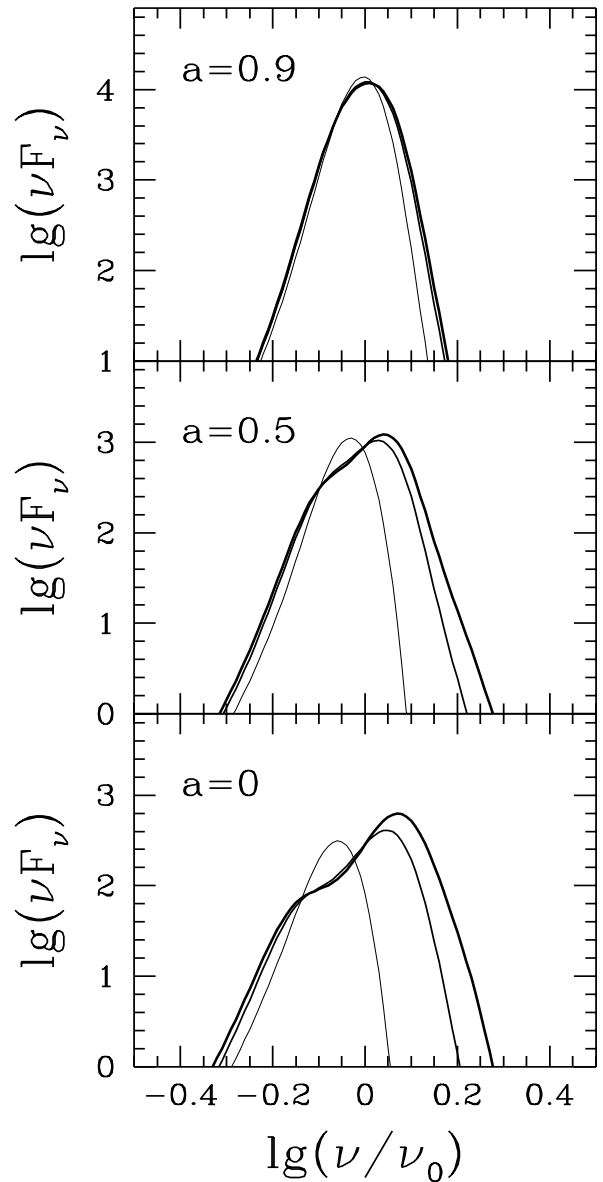


**Fig. 6.** The hypothetical line profiles emitted by our models for observers at inclinations  $\theta = 5^\circ$  (thin solid lines),  $60^\circ$  (medium lines), and  $85^\circ$  (thick lines). The three panels correspond to the three models as indicated. The flux units are arbitrary.

to the close vicinity of the equatorial plane. We obtain the three dimensional description of the flow assuming that the flow is quasi-spherical (we neglect the component  $u^\theta$  of the velocity) and that the density falls in the vertical direction as in isothermal atmosphere, with a constant scale height depending only on radius.

The influence of the relativistic effects in light propagation on the shape of the continuum spectra of advection dominated accretion flows seems to be marginal. This is due to the fact that the emitted spectra are very broad and the small frequency shifts are hard to distinguish.



The most important effect we find is the anisotropy of the radiation emitted from the disk, which favors observers near the equatorial plane. Observers close to this plane can see part of the matter as approaching them with the relativistic speed due to the combined effects of rotation and fast radial fall. This effect can be stronger than the occurrence of hot spots on the surface of thin Keplerian disk in the places approaching the observer with the highest velocity (Luminet 1979; Jaroszyński, Wambsganss & Paczyński 1992). Since matter is transparent one can see the beaming of radiation regardless of the place of its emission. The fact, that the effect is stronger in our models with slowly rotating holes is due to the different angular momentum distributions in the accreting matter. Also the fact, that the flow on the fast rotating hole ( $a = 0.9$ ) has a higher ion temperature (see the plots of the sound speed on Fig.1) has an impact. Since the electron temperature does not grow with ion temperature indefinitely but saturates at about  $10^{10}\text{K}$ , it makes the central, fast rotating part of the flow relatively less important as a source of radiation and relativistic effects become weaker than usually expected for a fast rotating hole.

The shape of the hypothetical  $\gamma$ -ray line, which we calculate, does not have a two-peak structure due to the superposition of photons coming from the different parts of the flow. The specific production mechanism of the line, which we use, also acts as to make the relativistic effects less pronounced. The cross-section for the lithium and beryllium production decreases with the ion temperature. The hotter flow on the Kerr hole with  $a = 0.9$  produces a stronger line, since the volume with the temperature above the threshold is larger, but in the same time, the central region is much less important.

In the conclusion we state, that the kinematics of advectively dominated accretion flows is difficult to investigate on the basis of spectral observations, since the possible pronounced spectral features are lacking. Also the parameter space of the possible ADAFs is much larger than in the case of Keplerian disks, which makes the task even harder.

*Acknowledgements.* We thank Jean-Pierre Lasota and Marek Abramowicz for the discussions concerning ADAFs, and one of us (MJ) for their kind hospitality during his visits to Meudon and Götheborg. This work was supported in part by the Polish State Committee for Scientific Research grant 2-P03D-020-08.

## References

- Abramowicz, M.A., Lasota, J.-P. & Xu, C., 1986, in *IAU Symposium 119, Quasars*, eds. Swarup, G. & Kapahi, V.K., Reidel, Dordrecht, p. 376  
 Abramowicz, M.A., Czerny, B., Lasota, J.-P. & Szuszkiewicz, E., 1988, *ApJ*, 332, 646  
 Abramowicz, M.A., Chen, X., Kato, S., Lasota, J.-P. & Regev, O., 1995, *ApJ*, 438, L37  
 Abramowicz, M.A., Chen, X., Granath, M. & Lasota, J.-P., 1996, *ApJ*, 471, 762 (ACGL)

- Abramowicz, M.A., Lanza, A. & Percival, M.J., 1997, to appear in *ApJ*, April 10 issue (ALP)  
 Bardeen, J.M., 1973, in *Black Holes*, eds. DeWitt, C. & DeWitt, B.S., Gordon & Breach, New York, p. 215  
 Begelman, M.C., 1978, *MNRAS*, 184, 53  
 Begelman, M.C., 1979, *MNRAS*, 187, 237  
 Begelman, M.C. & Meier, D.L., 1982, *ApJ*, 253, 873  
 Björnsson, G., Abramowicz, M.A., Chen, X. & Lasota, J.-P., 1996, *ApJ*, 467, 99  
 Chen, X., Abramowicz, M.A. & Lasota, J.-P., 1997, *ApJ*, 476, 61  
 Esin, A.A., Narayan, R., Ostriker, E. & Yi, I., 1996, *ApJ*, 465, 312  
 Hameury, J.-M., Marck, J.-A. & Pelat, D., 1994, *A&A*, 287, 795  
 Jaroszyński, M., 1993, *Acta Astron.*, 43, 183  
 Jaroszyński, M., Wambsganss, J. & Paczyński, B., 1992, *ApJ*, 396, L65  
 Jones, F.C., 1968, *Phys. Rev.*, 167, 1159  
 Katz, J.I., 1976, *ApJ*, 215, 265  
 Kozlovsky, B. & Ramaty, R., 1974, *ApJ*, 191, L43  
 Lasota, J.-P., 1994, in *Theory of Accretion Disks 2*, eds. Duschl, W.J., Frank, J., Meyer, F., Meyer-Hofmeister, E. & Tscharnuter, W.M., Kluwer Academic Publishers, Dordrecht, p. 341  
 Lasota, J.-P., Abramowicz, M.A., Chen, X., Krolik, J., Narayan, R., Yi, I., 1996, *ApJ*, 462, 142  
 Luminet, J.P., 1979, *A&A*, 75, 228  
 Narayan, R., 1996, *ApJ*, 462, 136  
 Narayan, R. & Yi, I., 1994, *ApJ*, 428, L13  
 Narayan, R. & Yi, I., 1995, *ApJ*, 452, 710  
 Narayan, R. & Yi, I., 1996, preprint astro-ph/9611008, submitted to *ApJ*  
 Narayan, R., McClintock, J.E. & Yi, I., 1996, *ApJ*, 457, 821  
 Novikov, I.D. & Thorne, K.S., 1973, in *Black Holes*, eds. DeWitt, C. & DeWitt, B.S., Gordon & Breach, New York, p. 343  
 Paczyński, B. & Wiita, P.J., 1980, *A&A*, 88, 23  
 Peitz, J. & Appl, S., 1996, submitted to *MNRAS*  
 Rees, M.J., 1982, in Riegler G., Blandford, R.D., eds., *The Galactic Center*, Am.Inst.Phys., New York, p. 166  
 Shakura, N.I. & Sunyaev, R.A., 1973, *A&A*, 24, 337  
 Shapiro, S.L., Lightman, A.P. & Eardley, D.M., 1976, *ApJ*, 204, 187  
 Svensson, R., 1982, *ApJ*, 258, 338